PROCESSING EFFECTS ON l/F NOISE AND OTHER DATA ARTIFACTS

James H. Wise
Jet Propulsion Laboratory

5/14/94

1 INTRODUCTION

There are many sources that can limit the usefulness of dynamic measurements, including detector noise, amplifier noise and various background environmental noise sources. Other noise can be generated system wide where high gain is required, such as 1/f noise in m gravity (μg) measurements. It is characterized by noise that falls off at approximately six dB per octave, which is a rate inversely proportional to frequency. An apparent noise source, which can be similar in appearance, is DC leakage into the lower frequency side lobes of each filter bin which is a function of the side lobes in the weighting function. A judicious choice of processing parameters can suppress the data artifacts and enhance data signal to noise ratio and resolution. This paper addresses these two and other processing parameters and shows how data can be improved when processing both static and fractional Hz dynamic signals in the same data, where capacitive coupling is inappropriate.

1/f random noise (as opposed to DC leakage) is independent of the desired signal and is unique to each data channel, in other words, is incoherent with I/f noise in other data channels, By using the intrinsic 1/f noise incoherence of two data channels for acquiring and processing data at lower frequencies and amplitudes, useful data can be obtained where they were hidden by conventional data processing methods, I/f noise can be further minimized in the lowest frequency bins by choosing weighting. functions with the lowest side lobes. DC leakage noise is coherent by definition, and can bc minimized by developing more accurate and stable DC compensation signal conditioners.

The data presented in this paper is illustrated using accelerometers sensitive toμg sources. The technique applies to any type of very high gain, low and fractional frequency transducer and signal conditioner system.

2 BACKGROUND

This paper was started comparing power spectral densities (PSDs) derived from coherent output power (COP) vs. cross spectral density (CSD), and then grew to include other artifacts. COP derived PSD's are deficient in their ability to properly define the PSI) as described in the appendix, a technical note on the subject. The only condition that provides a valid COP derived PSD is where incoherent input and transducer noise is non-existent and since the object is to suppress incoherent noise, the COP should not be used to process data for PSDs. The coherent signal will be corrupted by any incoherent input and transducer noise. COP is gaining wider use, however it is subject to misuse by all but the most knowledgeable who fully understand, recognize, and have the ability to

KEYWORDS: I/f noise suppression, DC leakage, *power* spectral density, cross *spectral* density, coherent output power, weighting functions, overlapped processing, resolution bandwidth

correct or compensate for the influence of noise sources, reverberation effects, input-output lime delay errors/feedback/non-linearities, interference, correlation effects, common source periodicities, and statistical sampling errors. These influences and COP in general are discussed in depth in Reference 1. It is strongly suggested reading for those who perform and use COP processed data.

AlIan Piersol prepared the appendix for me to verify my original concern abet.n the COP method which has been used at other facilities. It mathematically proves the validity of CSD derived PSD's described in this paper and verifies 1/f noise suppression using cross spectral density techniques. For a full understanding of the concept, it is essential to read the appendix before continuing.

3 DATA ACQUISITION ANI) PROCESSING SYSTEMS

Commercial high sensitivity servo-accelerometers were purchased and commercial signal conditioners were developed to buck out the earth's gravitational field. At the same time a unique JPL seismic isolation system was developed (Figure 1). Data acquisition and processing systems were assembled (Figures 2 and 3) and the data in Figures 4 through 12 are the result,

Two Sundstrand model QA 3000-20 accelerometers were mounted adjacent to each other on a metal plate placed on the platform of a JPL designed seismic isolation system (see Figure 1). One accelerometer could have been mounted on top of the other, but it would require fabricating a special mounting block, and the data wave length of interest is long compared to the dimensions of the test transducers. Only negligible errors are expected from this arrangement, The net suspension is composed of bungee cord. The system is relatively soft in the vertical direction and relatively stiff horizontally.

Seismic accelerations transmitted through the seismic isolation system were measured in the test. Two new design Dynamics (division of Waugh Controls) signal conditioners, model 7600A, were used to condition and provide the very high gain necessary to obtain a usable signal, The signal conditioners have the advantage of automatically compensating for the earths gravitational field when calibrating and making microgravity (µg) measurements in the laboratory. Use of this technique is not restricted to the laboratory, however, and may be used in other applications. The data acquisition system included Precision Instruments elliptic anti-aliasing filters, model 6612A-B-LP8, and a Visidaq model HP64 analog to digital converter (ADC) and storage system as shown in Figures 2 and 3. Data were processed in a Sun Work Station data system using Synergistic Technology's "VAMP" software package.

4 l/F NOISE AND WEIGHTING FUNCTION COMPARISON

4.1 l/F PSD NOISE. Power *spectral* densities were plotted for the two accelerometer channels (Figures 4A and B) using a Harming weighting function whose first lobe is 32 dB below the peak. Both plots show a seismic frequency at 0.742 Hz and identical amplitudes. As expected, comparison of the two PSD channels reveal different amplitudes and some frequency distribution differences in the frequency range of the l/f noise, but not in the frequency range of the seismic data signal.

A slight difference in the measured overall root mean square (RMS) amplitudes (channel 1: 4.969 $\mu g^2/Hz$ and channel 2:4.933 $\mu g^2/Hz$) can be attributed to these same differences in the l/f noise for each channel. These differences are caused by imperfect gravitational field zeroing and less than infinite averaging, in the two channels in this region, Increasing the number of averages should increase the incoherent I/f noise suppression

I/f noise in channel 1 is greater than channel 2 as shown by comparing Figures 4A and B. An examination of Figures 4D E and F clearly demonstrate l/f noise incoherence. In the 1/f frequency range, the magnitude of the frequency response function (commonly referred to as the transfer function) approaches zero and fluctuations in phase response, indicate incoherency. The only real proof is shown by the coherence function, which approaches zero. If the coherent seismic signal were not present to mask it, these data could show incoherence to perhaps 2 Hz or higher.

4.2 **1/F PSDs FROM CSDs.** This section shows how reduction of 1/f noise is obtained by use of the CSD to obtain the PSD. This is a feature which demonstrates two important attributes of this technique: I/f noise is minimized as expected, and the use of the CSD to obtain the PSD does not affect the desired coherent signal. In order to maximize l/f noise suppression, the number of averages should be increased. Overlapped processing can be used to reduce data acquisition time at these low frequencies but there is a price to pay and the pro's and con's are discussed in section 4.4 of this paper.

When two transducers measure the same dynamic excitation at the same location, the magnitude of the CSD derived PSI) is identical to a PSD from a single transducer. Assuming no extraneous noise, the appendix defines the CSD and coherent output power (COP) and their ability to provide a meaningful 1/f noise suppressed PSI) while a valid PSD is obtained for the desired coherent signal. Figure 4C is a plot of the CSD derived PSD from the same time history as the PSD's in Figures 4A and B. CSD 1/f noise reduction is greater than one decade below the PSD for channel 1 noise and approaches a decade below channel 2 noise. If the seismic signal at 0.742 Hz were not present it is expected that the data would show I/f noise to continue dropping off at the same approximate rate of six dB per octave to perhaps 2 Hz where intrinsic system noise would mask l/f noise. If data acquisition time of the two channels is insufficient, the result is only partial l/f noise compensation. This can be seen by examining I/f noise in Figures 4A and B and noting that only partial noise suppression has been achieved in the PSD derived from the CSD in Figure 4C. Increased averaging time should improve incoherent noise suppression.

Further evidence of incoherence in the CSD I/f noise is displayed by Figures 4D, E, and F. Figure 4D is the frequency response function magnitude which is lower in the frequency range of the l/f noise than either single channel derived PSD. Figure 4E is the frequency response function phase between channels 1 and 2. Phase exhibits wild fluctuations in the range of 1/f noise because of it's incoherence. Figure 4F is the coherence function which is significantly reduced in the same range and proves incoherence. Figures 4D, E, and F verify the incoherence of l/f noise in the two data channels and proves the validity of this technique.

4.3 EFFECT OF DIFFERENT WEIGHTING FUNCTIONS. The data in Figures 4A through F were processed with a Harming weighting function whose first lobe is down 32 dB from the peak

of the frequency bin, and each successive lobe falls off at a rate of 18 dB per octave. Figures 5A, B and C are the same data as Figures 4A, 13 and C except a Kaiser-Bessel weighting function was used, whose first side lobe is at least 70 dB below the peak of the frequency bin. Figure 5C shows the PSD using the CSD technique and Kaiser-Bessel weighting, This window is the only one in the VAMP system which can show the effect of lower side lobes on the slope of I/f noise. Unfortunate] y, the Kaiser-Bessel weighting function leads to a wider noise bandwidth than the Harming weighting function, thus reducing it's ability to resolve fine data structure. Using a boxcar weighting function (actually, no weighting at all) as a reference, the Hanning function noise bandwidth is 1.5 times the boxcar weighting function, while the Kaiser-Bessel is 1.8, Other weighting functions might prove to be a better choice. In spite of the wider noise bandwidth of the Kaiser-13 essel weighting function, the significantly lower side lobes provides a marked improvement in incoherent 1/f noise suppression compared to Harming weighting.

An examination of all plots comparing l/f noise in the same frequency range, time frame, and filter bandwidth (Figures 4 and 5, and Figures 6 and 7) shows that the coherent seismic signal at 0,742 Hz remains unchanged while the incoherent I/f noise is suppressed. This clearly demonstrates that incoherent noise is reduced, while the coherent signal is unaffected when obtaining the PSD from the CSD. Serious erroneous decisions can be made if the COP is used to produce the PSD.

A comparison of CSD weighting function data shows the l/f noise slope beyond the first filter bin is steeper with a Kaiser-Bessel weighting function than with the Harming weighting function (compare the levels at 0.02 Hz in Figures 4C and 5C) which indicates that some of the noise is due to leakage of the DC component into the lobes of adjacent filter bins. The only way to differentiate between the obviously coherent DC leakage in the low frequency lobes and the incoherent l/f noise is with the coherence function (Figures 4F and 5F). The higher side lobes of the Harming weighting function cannot suppress the l/f noise as efficiently as the Kaiser-Bessel weighting function. Weighting functions with the lowest side lobes must be used to obtain maximum suppression of incoherent l/f noise,

The greater CSD coherence at frequencies close to DC with a Kaiser-Bessel weighting function (compared to the Harming fiction) substantiates the premise that this data is not solely due to I/f noise, but is also a function of DC noise leakage into *the* side lobes of the lowest frequency bins. If l/f noise were to continue to DC, the noise would be a function of 1/0 Hz, or infinite. Since this obviously does not occur, at some point l/f noise can be assumed to have a "knee" where it falls off as zero Hz is approached. Evidence of this "knee" can be seen in Figures 5 and 7A, 13, and C. A narrower bandwidth analysis than is available at JPI, is desirable to pursue this to lower frequencies, Theoretically, I/f noise can reach O Hz, but this concept applies to obscure examples and does not apply to concepts in this paper. See Reference 2 for more information,,

Noise which has historically been described as l/f noise is shown in this data to be a combination of l/f noise and DC leakage into filter bin side lobes even when a very small DC component exists. In the unlikely event that the DC component is non-existent, leakage will not occur. DC leakage can occur not only from a gravitational field, but also from signal conditioning bias. An examination of the coherence function of Figures 5 and 7F indicates that the 0.0025,0.005, and 0.0075 Hz freq-

uency bins all have a coherence of 1 which is due to DC leakage, while the frequency bin at 0.01 Hz drops to approximately 0,26 where the s1ow decreases rapidly due i/f noise incoherence. Compare the coherence functions of Figures 4F and 5F to see the effect different weighting functions have on what has traditionally been thought to be all l/f noise. DC leakage noise can be reduced if better and more stable DC compensation of signal conditioners can be achieved, Unfortunately, present economic conditions precludes funding the development of more accurate and stable DC compensation signal conditioners by JPL. We are grateful for the development of gravity compensated signal conditioners by Dynamics Instruments, which made data acquisition for this paper possible.

4.4 EFFECTS OF OVERLAPPED PROCESSING. Figures 6 and 7A through F show the results of Harming and Kaiser-Bessel windows and 75'%0 overlapped processing, The PSDs appear similar to those in Figures 4 and 5A, B, and C but there are some differences in the 1/f noise reduction in the overlapped single channel PSD and PSD's obtained from the CSD. Since the time period of the overlapped processing is 1/4 that of the non-overlapped processed data, this can be an artifact of the difference in processing time and random system noise fluctuations.

This illustrates another important data artifact, While the number of data samples is the same for n = 100 of the non-overlapped data as compared to the 3/4 overlapped data (Figures 4 and 6A through F), the overlapped time history is processed over only 1/4 of the non-overlapped time history. Data smoothing is equivalent, but since time in the formula for the number of statistical degrees of freedom (n = 2Bt) is a function of the length of the data sample, statistical confidence in the data is only 1/4 that of non-overlapped data, or n = 25. As a result, one should not expect the data to be identical.

When Figures 7A through F are compared with Figures 5A through F (both with Kaiser-Bessel weighting functions), similar differences can be observed,

5 EFFECTS OF RESOLUTION BANDWIDTH ON LOW FREQUENCY DATA.

All figures in this paper show digital data from the same start time. Figures 4 and 5 cover the same time durations, but the remaining figures are for shorter times due to their overlapped processing or wider frequency resolution, Note that the filter bandwidth of each plot is resolution bandwidth, not noise bandwidth, which is wider. As the filter noise bandwidth increases, details of fine data structure is lost because more peaks can be hidden within a single frequency bin. This practice makes the data look smoother, but hides it's true nature and makes narrow resonances appear wider, Data should be processed with a noise filter bandwidth at least 1/4 the data resonance bandwidth to properly resolve the data resonance,

These phenomena can plainly be seen by comparing the PSD's of Figures 4, and 5 A, B, and C with the progressively greater noise bandwidths as found in Figures 8A, B, and C through 12A, B, and C! with resolution bandwidths varying from 0.005 Hz to 0.1 Hz. The most dramatic comparison is to follow the resolution loss in the 0.745 Hz resonance peak from Figures 4 and 5 with the resolution in Figures 8 through 12 and the loss of fine resolution between 5 and 10 Hz in Figures 10, 11, and 12. This is particularly troublesome for dynamicists performing modal analyses.

6 COMMENTS AND CONCLUSIONS.

μg and similar high sensitivity and low and fractional Hz data should be processed with the narrowest frequency resolution consistent with available time constraints, weighting functions with the lowest side lobes, and PSDS calculated from the magnitude of the cross spectral density.

The data indicates that small DC leakage into the first frequency bin also leaks into the adjacent filter bin skirts causing the inverse relationship between frequency and magnitude close to the lowest frequency as seen in the CSD plots (Figures 4C and 5C). The. inverse relationship of noise and frequency indicates that this is true because of the increase in coherence at the lowest frequencies. If so, noise close to DC maybe lowered by a more accurate and stable DC compensation of the signal conditioners. The high coherence in the first three filter bins with Kaiser-Bessel weighting supports the theory that *noise is also caused* by DC leakage into the lobes of the filter bins, in addition to 1/f noise.

Weighting functions should bc examined and tested to minimize 1/f noise into the lowest filter bins. Different weighting functions may increase noise filter bandwidth by different amounts in addition to lower side lobes and some compromise may be in order to obtain optimum results.

The data shows that traditionally considered l/f noise is actually a combination of l/f noise and DC leakage into the lowest filter skirts. The slope of DC leakage noise can approximate the slope of 1/f noise, but can also deviate from a l/f slope. The slope of DC leakage noise is "a function of the amplitude of the first lobe and the slope of the filter skirts, which are a result of the weighting function (compare Figures 4C with SC and 4F with 5F).

If CSD data channel l/f noise averages can be increased a greater l/f noise reduction should be attained than that in Figures 4C and 5C. The data, however, proves the validity of the technique.

An examination of PSD and CSD data processed under the same parameters shows the coherent seismic signal obtained from the CSD to remain unchanged while the incoherent l/f noise is suppressed. This clearly demonstrates that incoherent noise is reduced, while the coherent signal is unaffected when obtaining the PSD from the CSD.

The length of data time required to process fractional Hz data can be prohibitive and overlapped processing can be a viable alternative. However, it should be remembered that statistical confidence is compromised.

The processes shown in this data promises to make extremely small and greater sensitivity (precision to 10-s μg) miniature accelerometers, currently under development at JPL, significantly more useful at frequencies below 2 Hz and very low magnitudes. Because of their small size and weight (estimated to be a few grams) a second transducer does not significantly add to the mass and stiffness of the item under test, compared with using single traditional transducers to obtain the PSD. In fact, the effect of using two miniature transducers on mass and stiffness will be less, compared to using the heavier single servo-accelerometers used in past years,

REFERENCES:

1, Bendat, J.S. and Piersol, A. G., Engineering Applications Of Correlation And Spectral Analysis, Wiley Interscience, 1993, Second Edition, Chapter 9

2. Bendat, J.S. and Piersol, A. G., Random Data: Analysis And Measurement Procedures, Wiley Interscience, 1971, First Edition, pp 73 and 75-82

ACKNOWLEDGEMENTS:

I thank Harry Himelblau and Allan Piersol for their comments and recommendations which enhanced the quality of the paper. In addition, Allen provided the appendix which is an unpublished technical note on the paper subject.

I thank Tony Zavala of JPL's Instrumentation Section for his expertise providing data acquisition, data processing, and figures for the paper.

APPENDIX

SUPPRESSION OF NOISE IN POWER SPECTRA MEASUREMENTS USING TWO TRANSDUCERS

AUTHORED BY ALLAN PIERSOL

SUPPRESSION OF NOISE IN POWER SPECTRA MEASUREMENTS USING TWO TRANSDUCERS

Assume an environmental signal u(t) is measured using two identical transducers mounted side-by-side so that both transducers measure u(t) precisely. Further assume both transducer signals are contaminated by extraneous instrumentation noise such that the actual measured signals from the two transducers are

$$x(t) = u(t) + m(t) \; ; \; y(t) = u(t) + n(t) \tag{1}$$

Finally, assume the instrumentation noise signals m(t) and n(t) are statistically independent of the environmental signal u(t), as well as one another (this is generally a valid assumption as long' as the instrumentation noise is not "microphonics" in nature). The power spectra for x(t) and y(t) are given by

$$G_{xx}(f) = G_{uu}(f) + G_{mm}(f) \; ; \; G_{yy}(f) = G_{uu}(f) + G_{nn}(f) \tag{2}$$

and from [1, p. 77], the cross-spectral density function between x(t) and y(t) is given by

$$G_{xy}(f) = G_{uu}(f) + G_{un}(f) + G_{um}(f) + G_{rin}(f) \tag{3}$$

However, under the stated assumptions,

$$G_{in}(f) = G_{um}(f) = G_{in}(f) = 0 \tag{4}$$

Hence, the cross-spectral density function between the signals x(t) and y(t) reduces simply to the power spectral density function of the environmental signal u(t); i.e.,

$$G_{xy}(f) = G_{uu}(f) \tag{5}$$

This is the basis for the common experimental procedure of making measurements with two closely spaced transducers to obtain noise-free power spectra estimates of an underlying signal:

Now consider the case where the coherent output power spectrum of y(t) on x(t) is computed by

$$G_{y:x}(f) = \gamma^2_{xy}(f) G_{yy}(f) \tag{6}$$

From [1, p. **181], it follows that**

$$G_{y:x}(f) = \frac{|G_{xy}(f)|^2}{G_{xx}(f)\,G_{yy}(f)}\,G_{yy}(f) = \frac{|G_{uu}(f)|^2}{G_{uu}(f) + G_{mm}(f)} = \frac{G_{uu}(f)}{1 + \dfrac{G_{mm}(f)}{G_{uu}(f)}} \qquad (7)$$

It is clear from Equation (6) that $G_{y:x}(f) \neq G_{uu}(f)$ except for the special case where $G_{mm}(f) = O$. Hence, under the stated assumptions, the coherent output power computation does not provide a meaningful quantity.

Reference

1. **Bendat,** J. S., and Piersol, A. G., *Random Data: Analysis and Measurement Procedures,* 2nd edition, Wiley, New York, 1986.

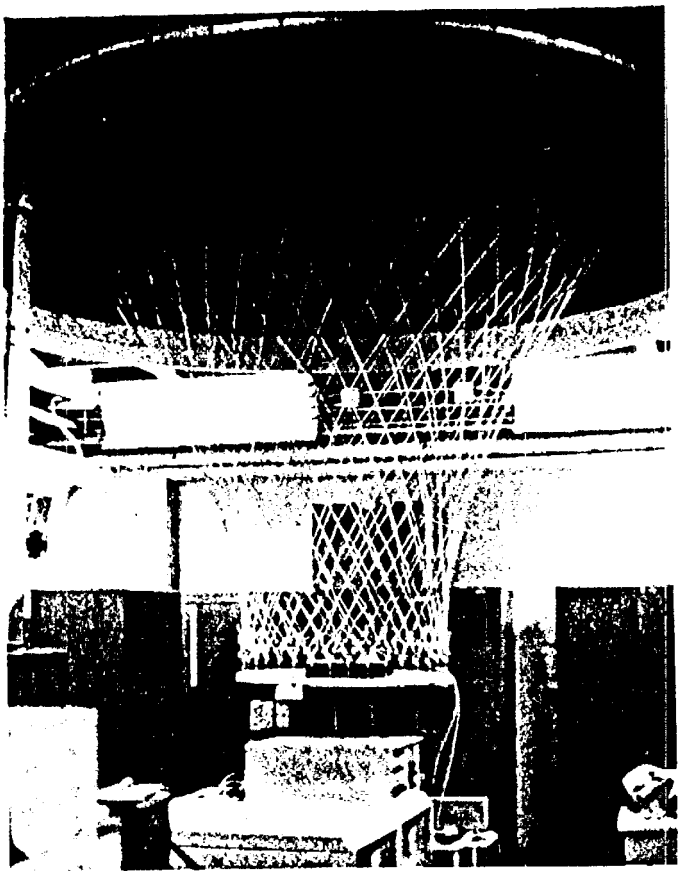

Figure 1A. **Seismic** Isolation Net

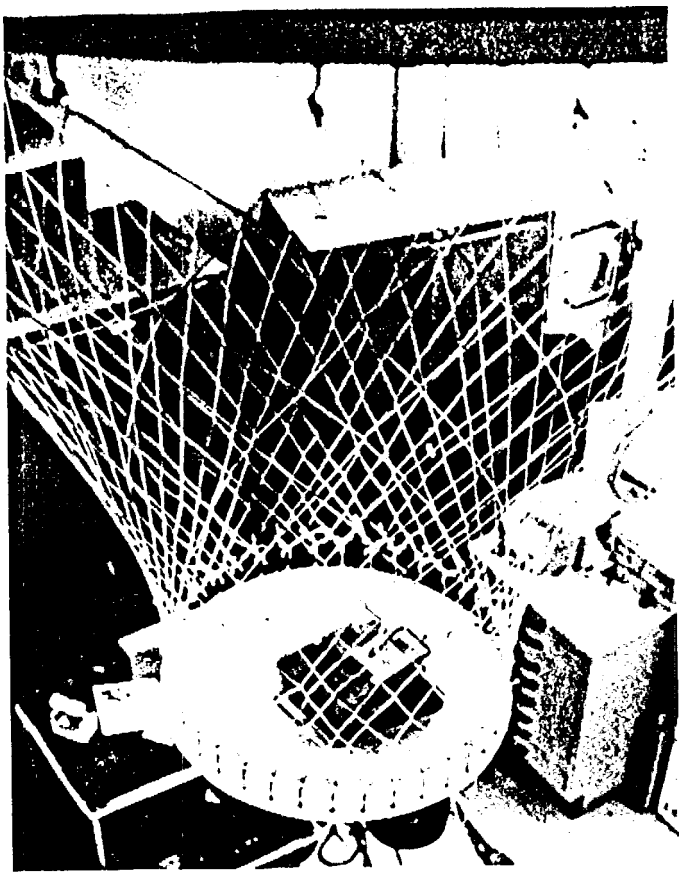

Figure lB. **Accels.** On Platform

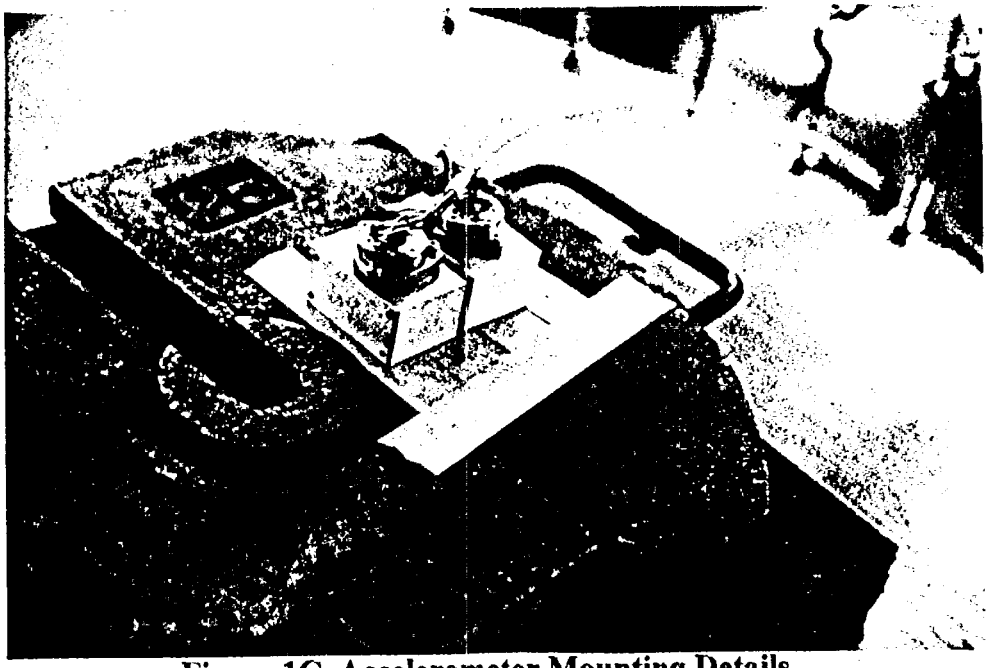

Figure 1C. Accelerometer Mounting Details

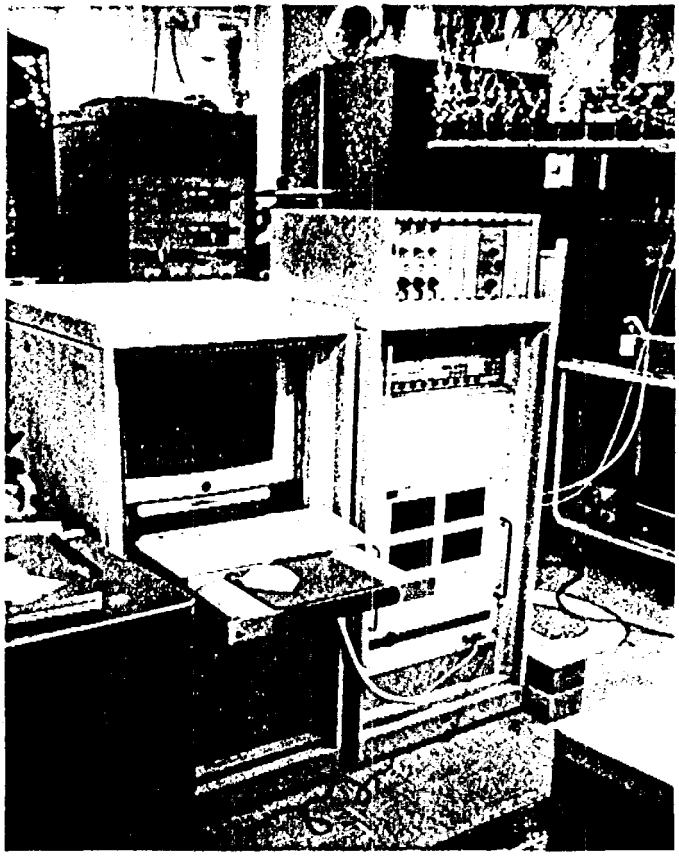

Figure 2A. Data Acquisition/Processing System

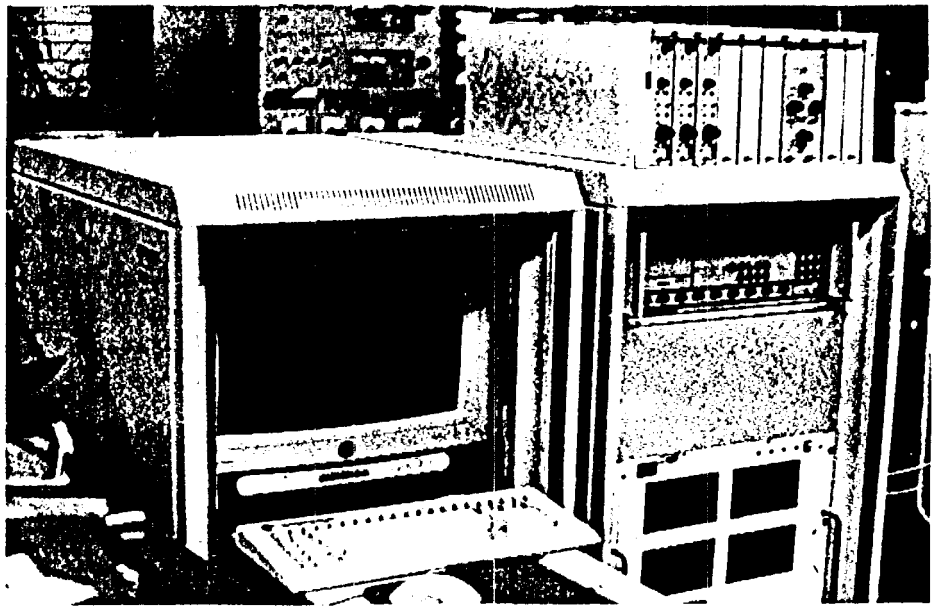

Figure **2B.** Data Acquisition/Processing System

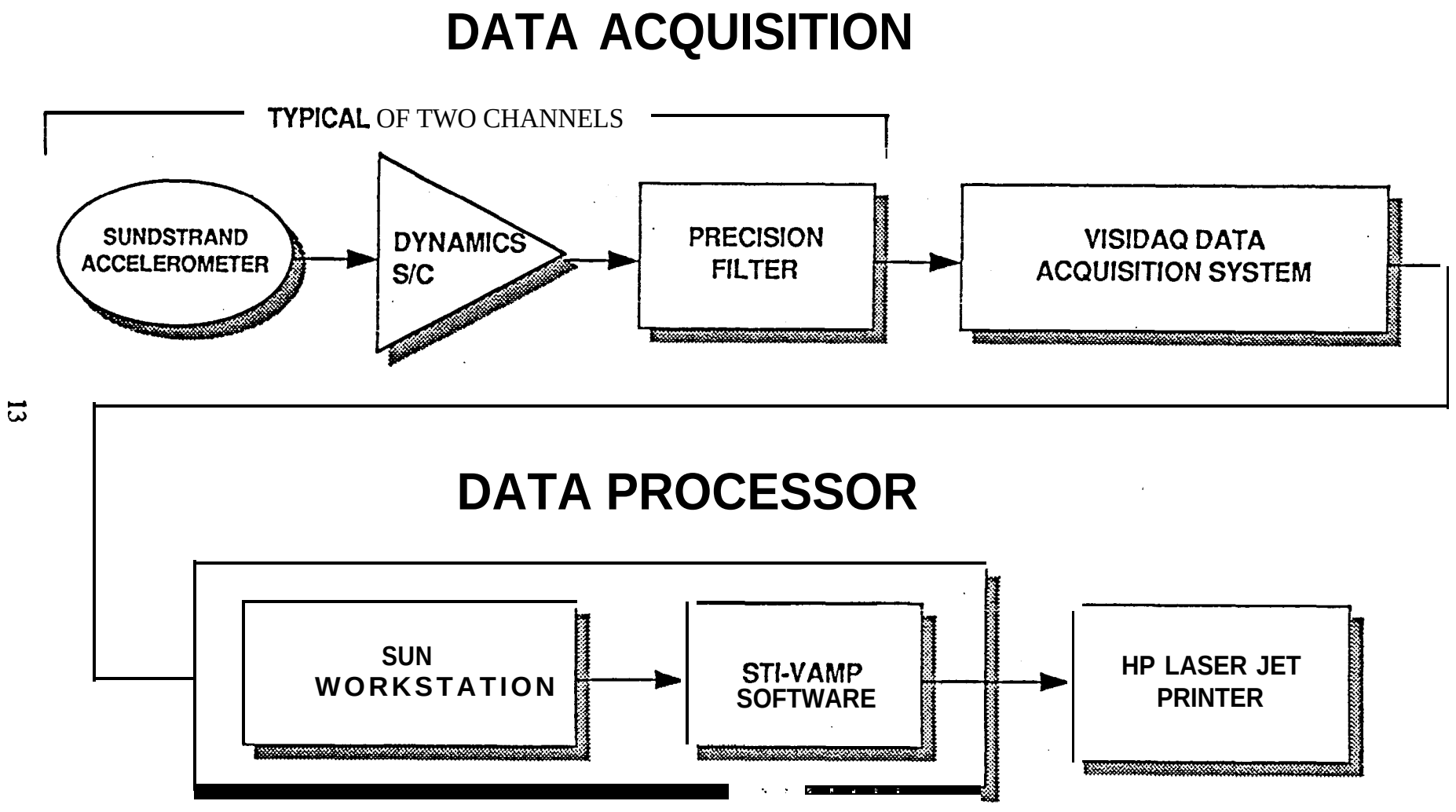

Figure 3. Data Acquisition/f? recessing System Block Diagram

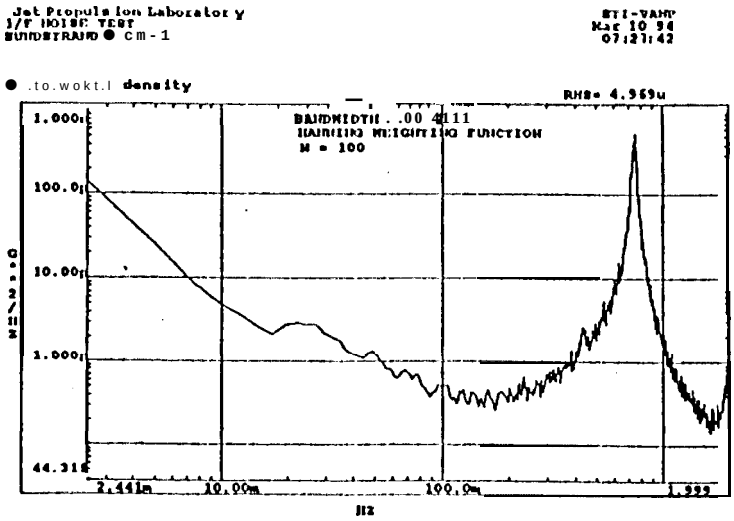

Figure 4A

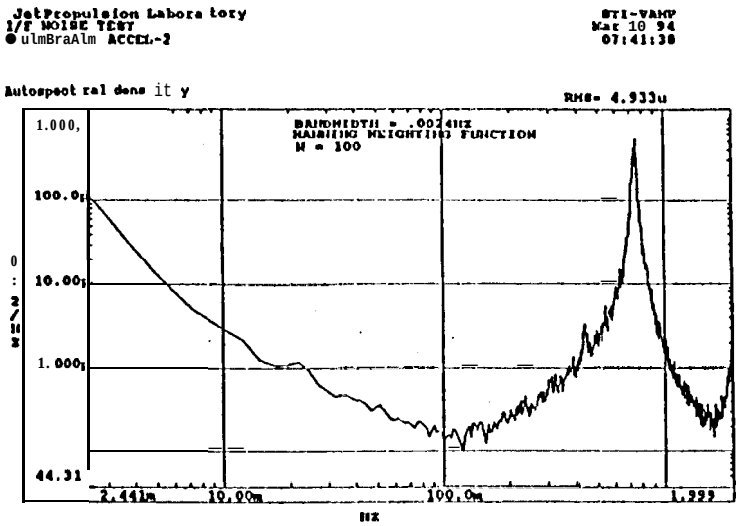

Figure 4B

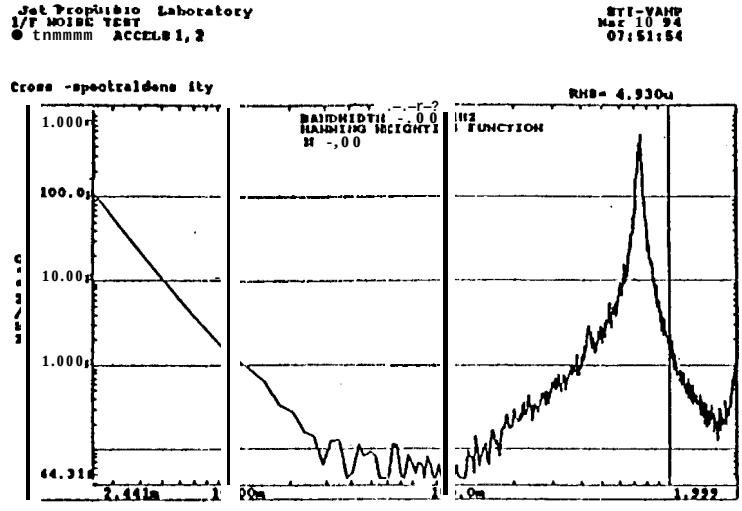

Figure 4C

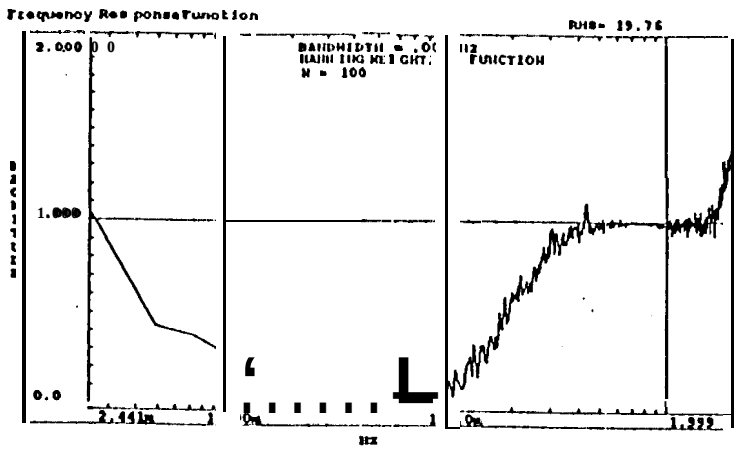

Figure 4D

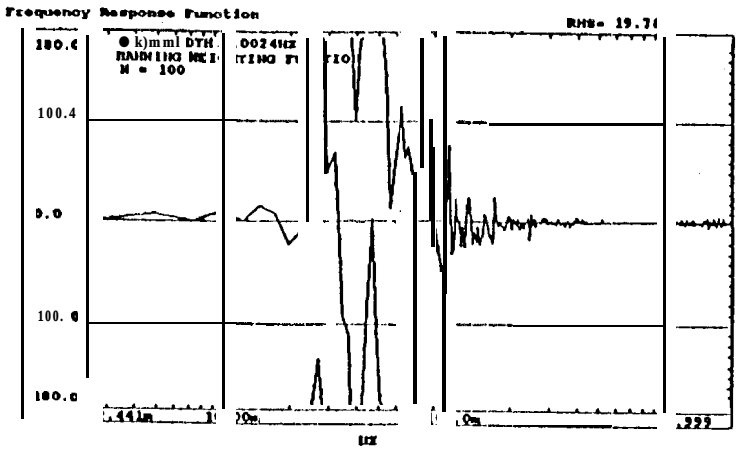

Figure 4E

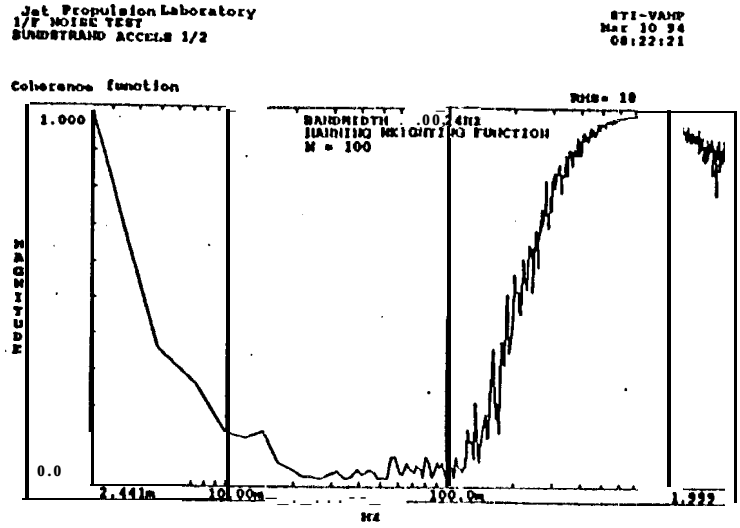

b"l@r941

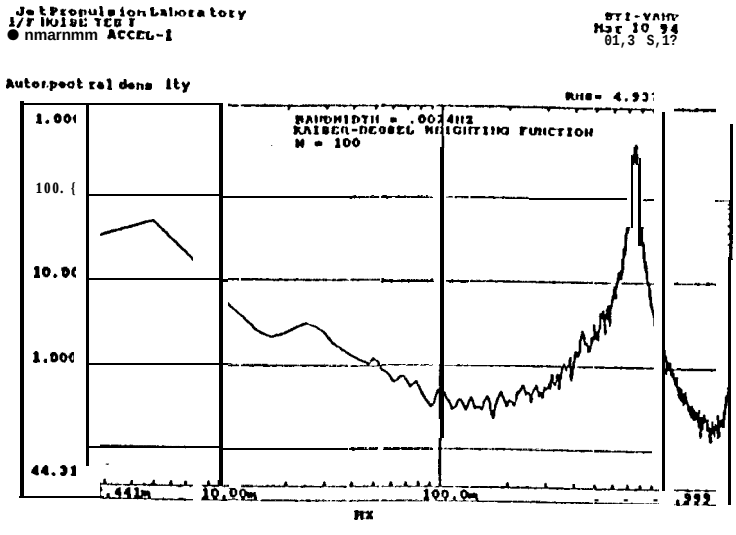

Figure 5A

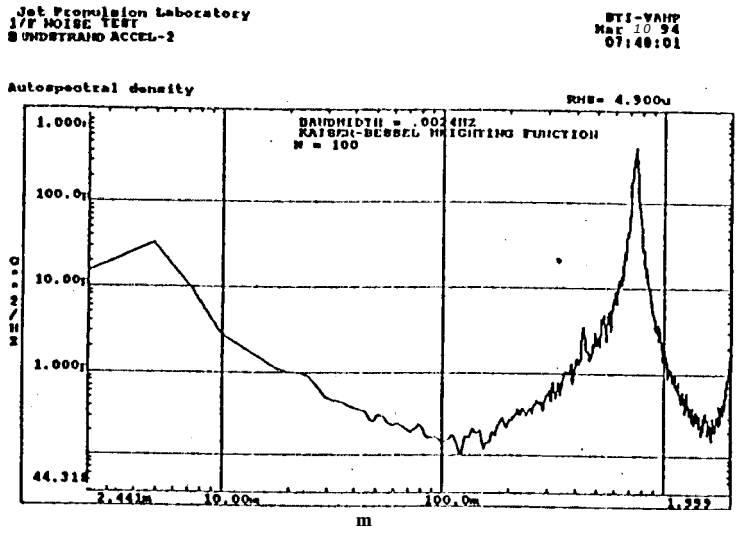

Figure 5B

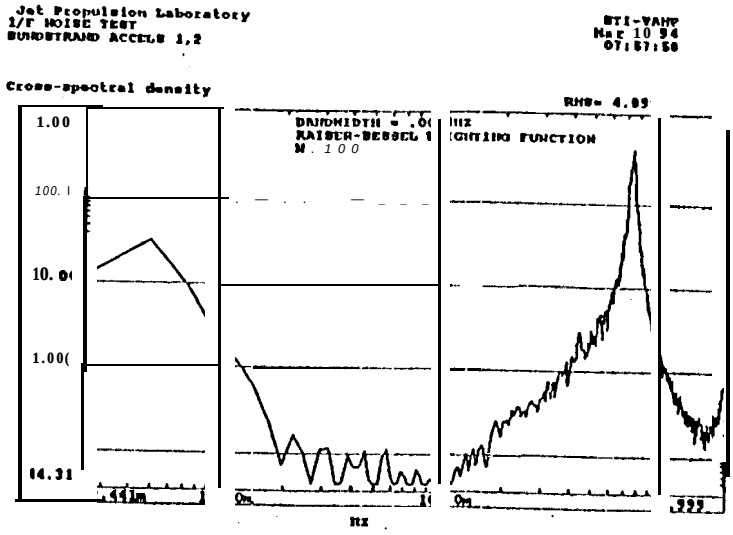

Figure 5C

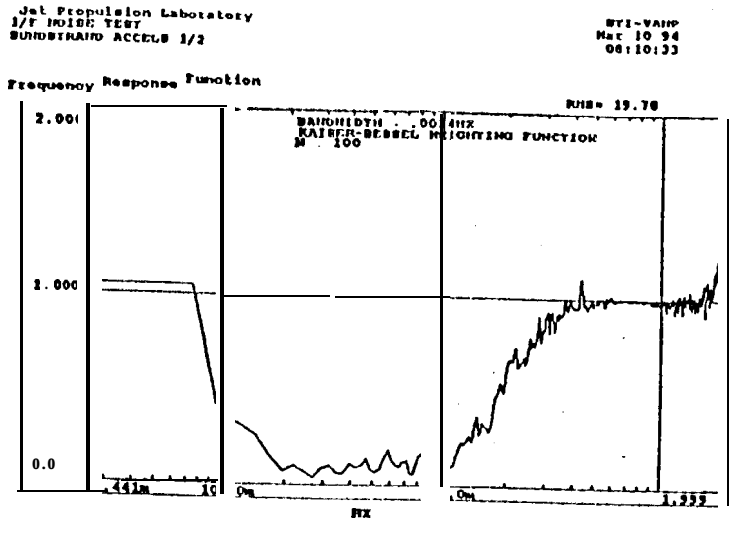

Figure 5D

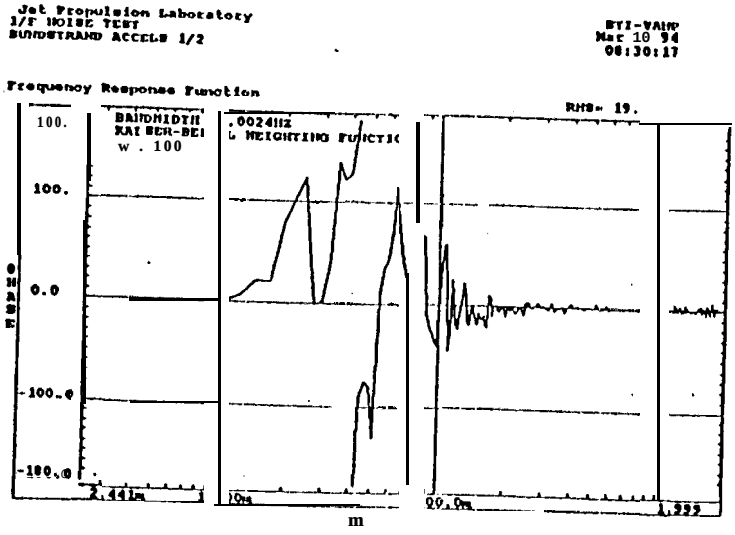

Figure 5E

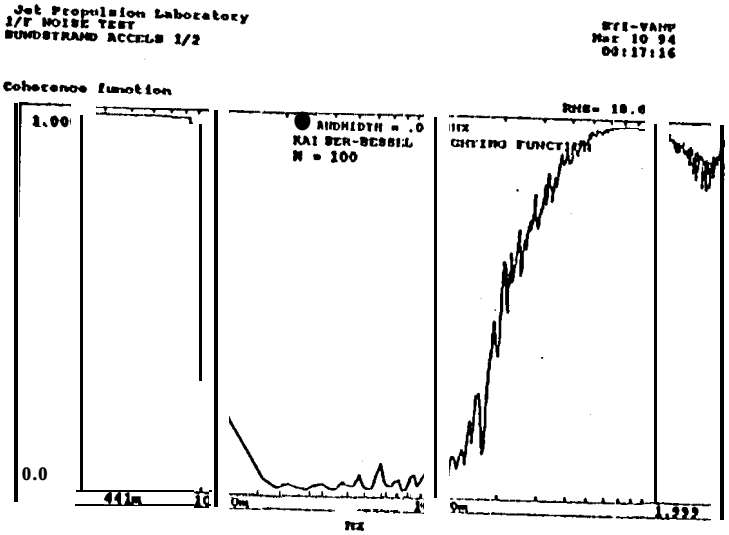

Figure 5F

1/F NOISE TEST
SUNDSTRAND ACCEL-1
07:31:31

Autospectral density

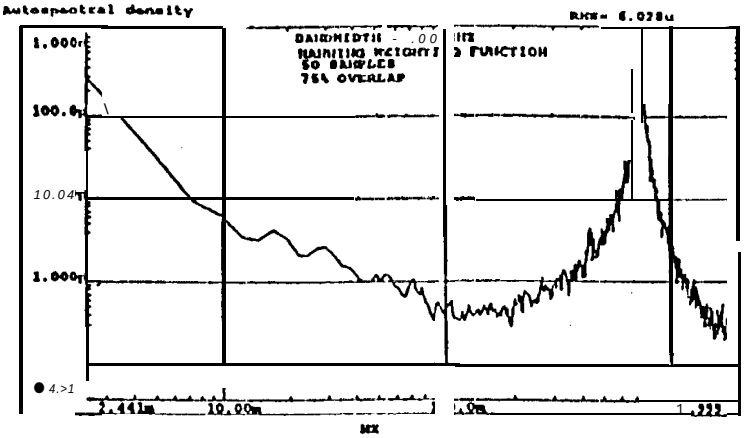

Figure 6A

Jet Propulsion Laboratory
1/F NOISE TEST
SUNDSTRAND ACCEL-2

STI-VAMP
Mar 10 94
07:44:46

Autospectral density

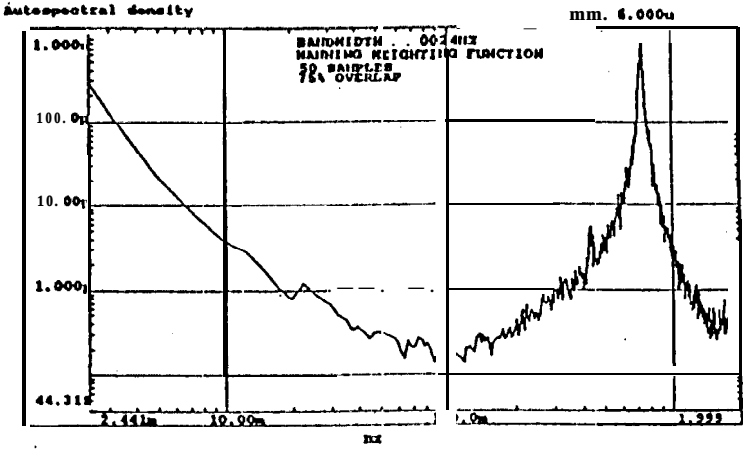

Figure 6B

JetPropulsion Laboratory
1/F NOISE TEST
SUNDSTRAND ACCELS 1,2

STI-VAMP
Mar 10 94
018s48s1

Cross-spectral density

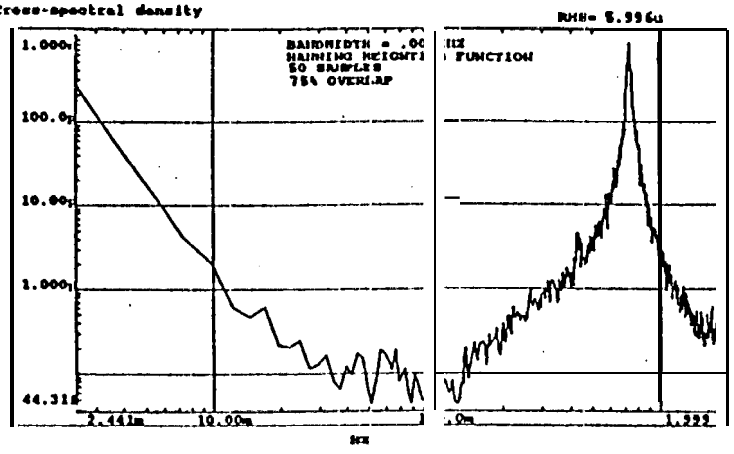

Figure 6C

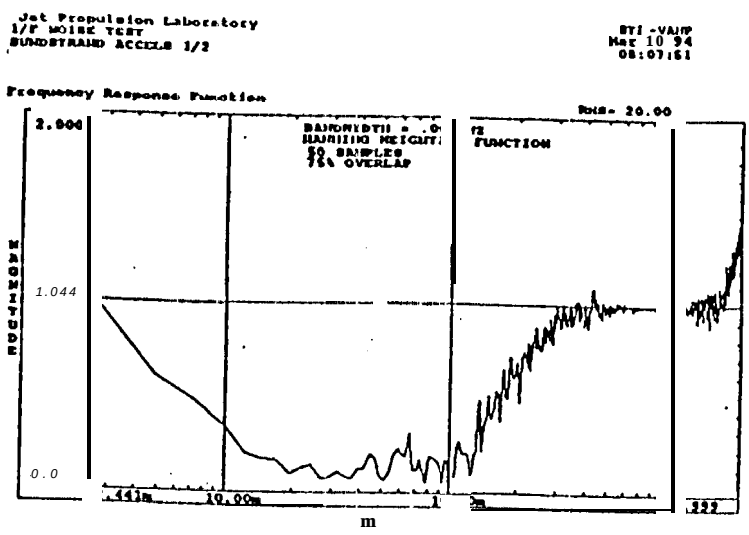

Figure 6D

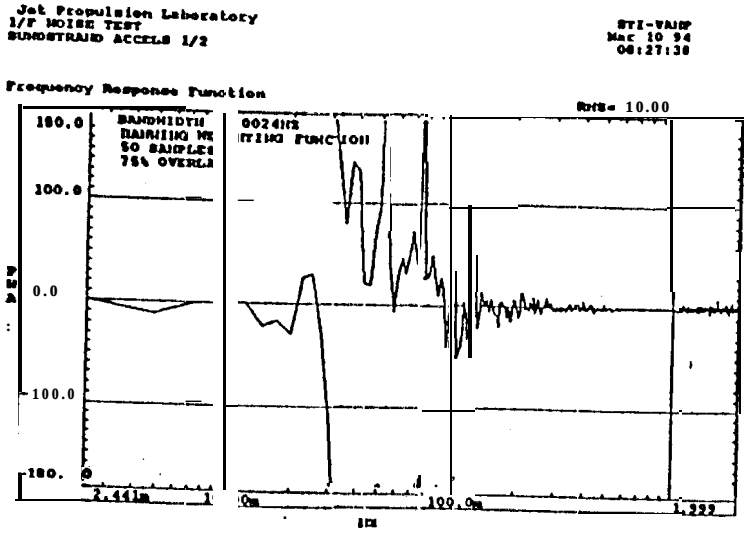

Figure 6E

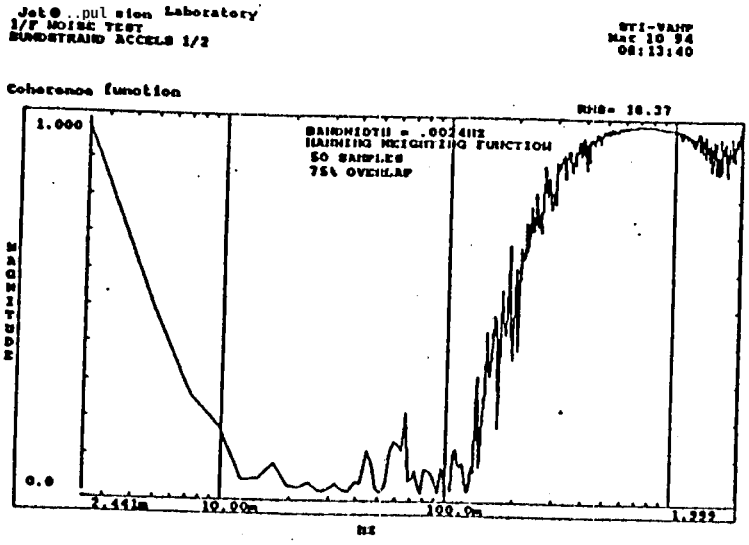

Figure 6F

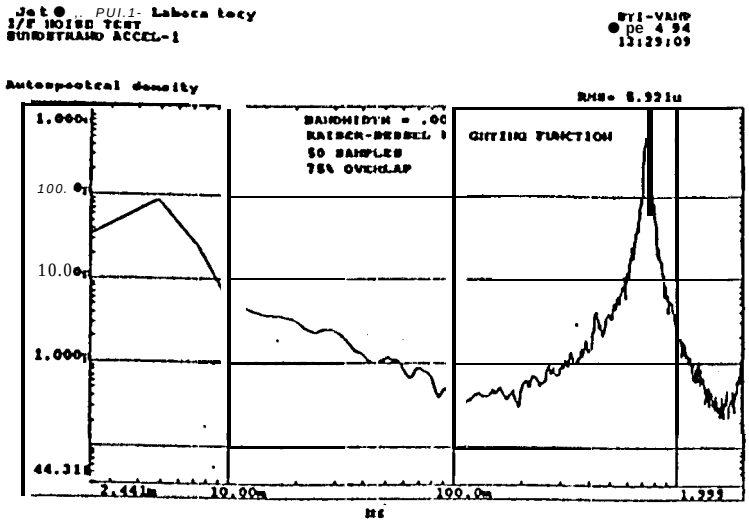

Figure 7A

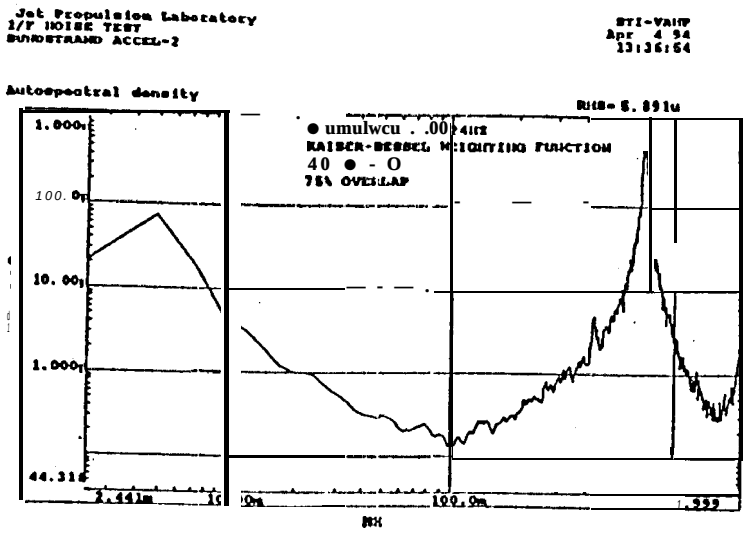

Figure 7B

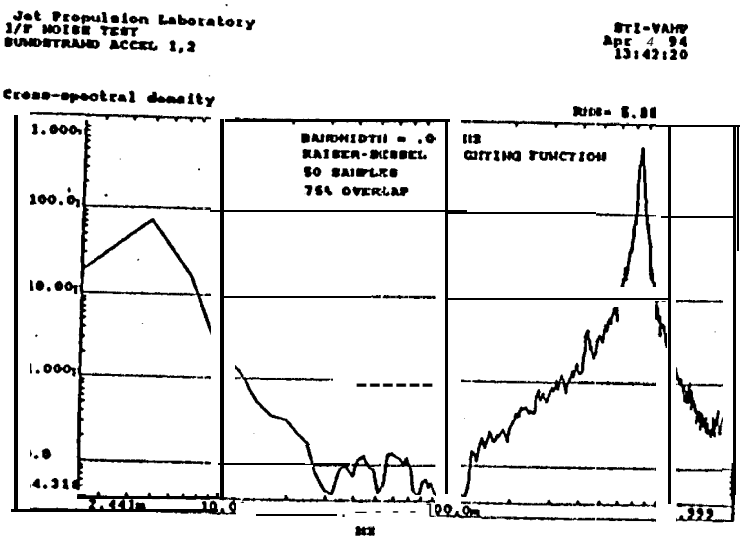

Figure 7C

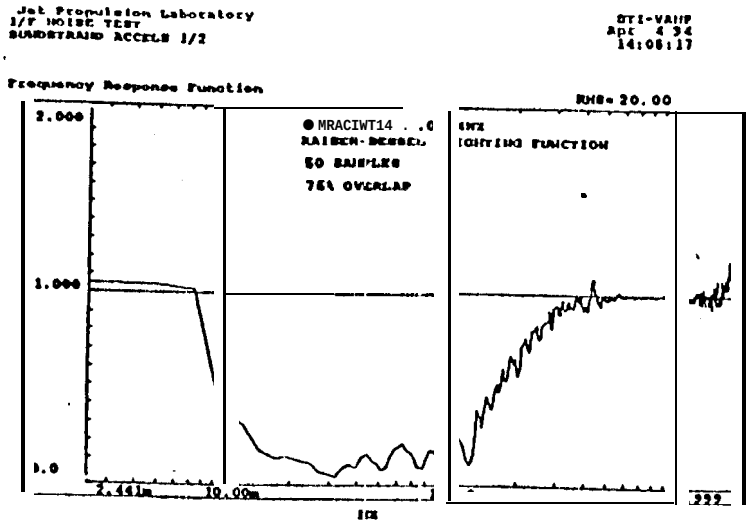

Figure 7D

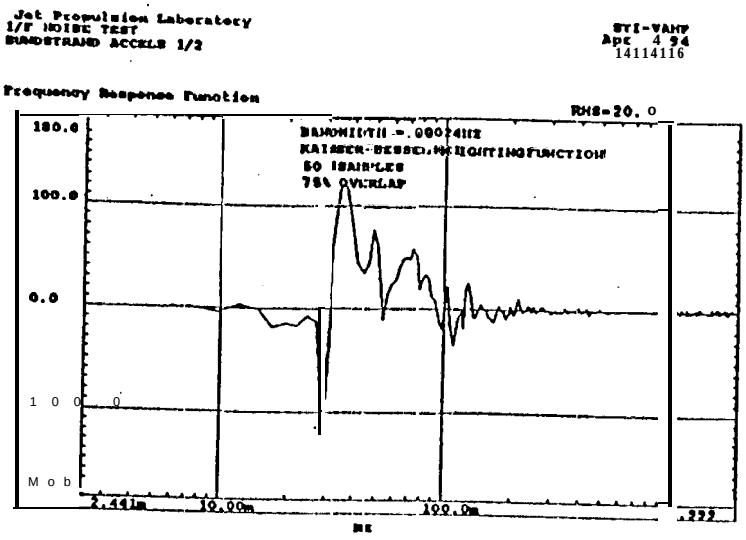

Figure 7E

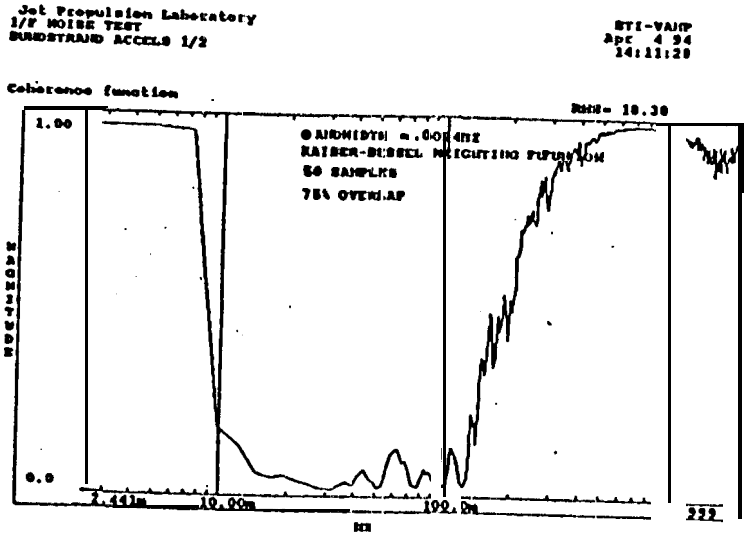

Figure 7F

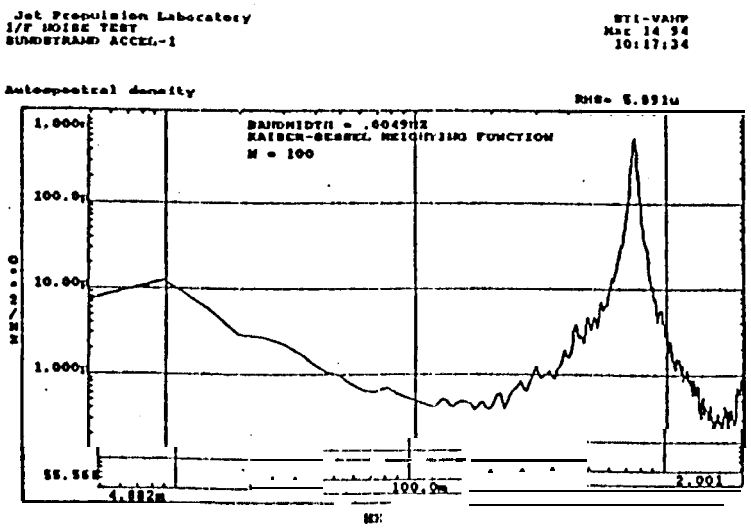

Figure 1A

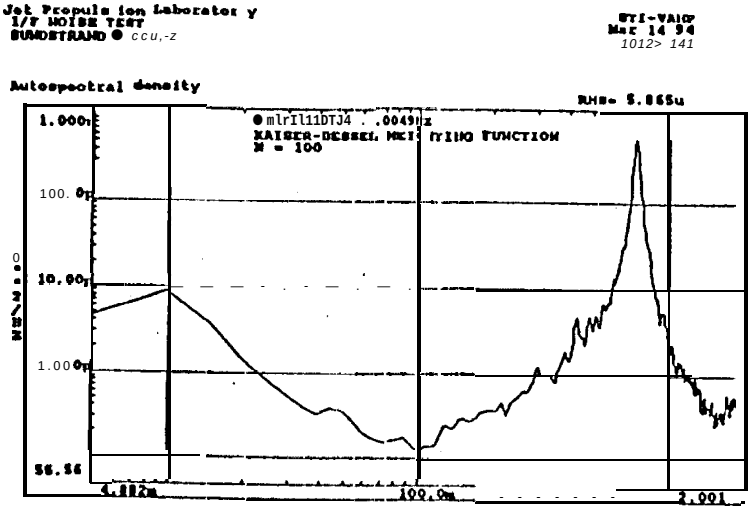

Figure 1B

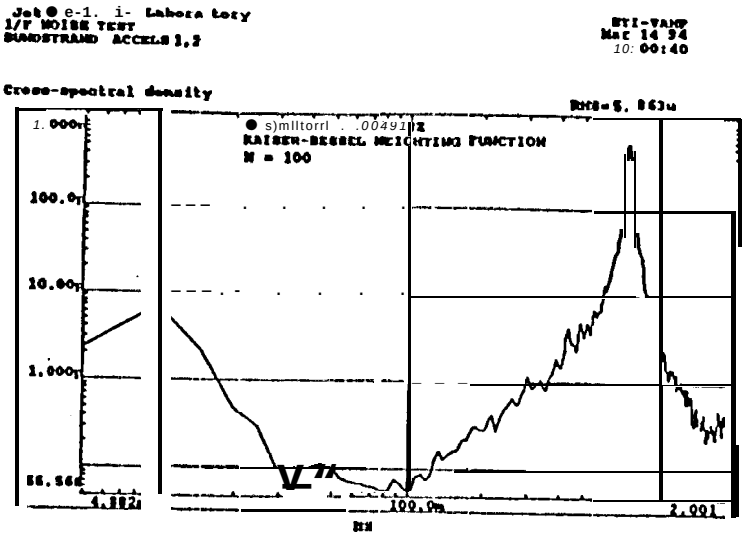

Figure 1C

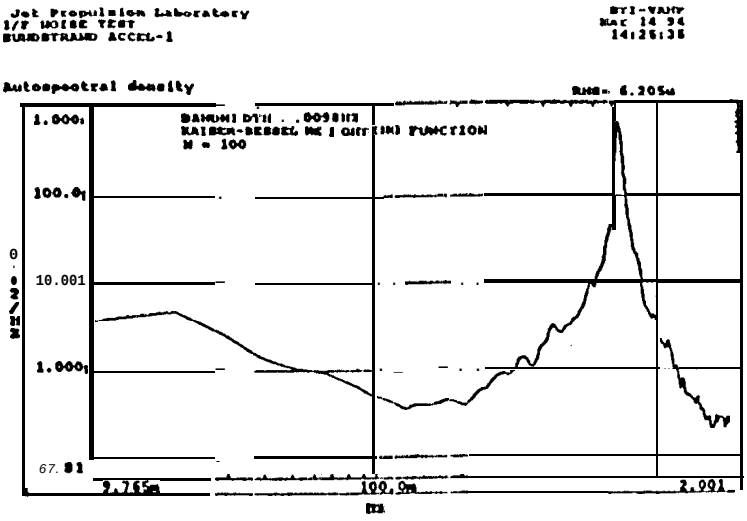

Figure 9A

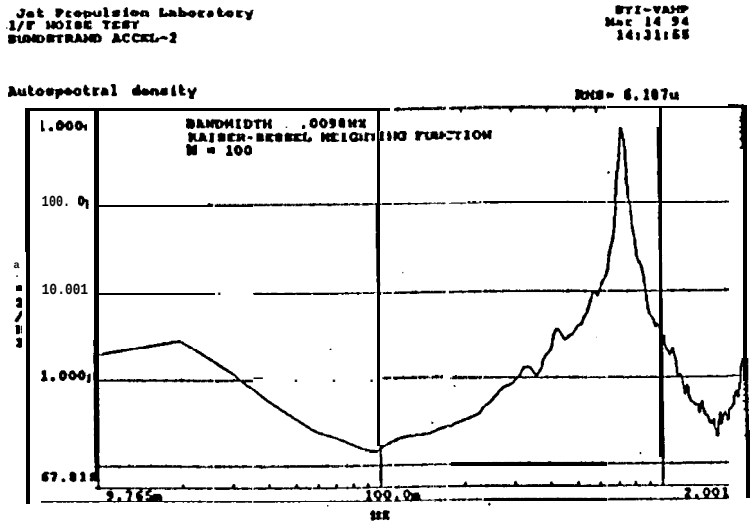

Figure 9B

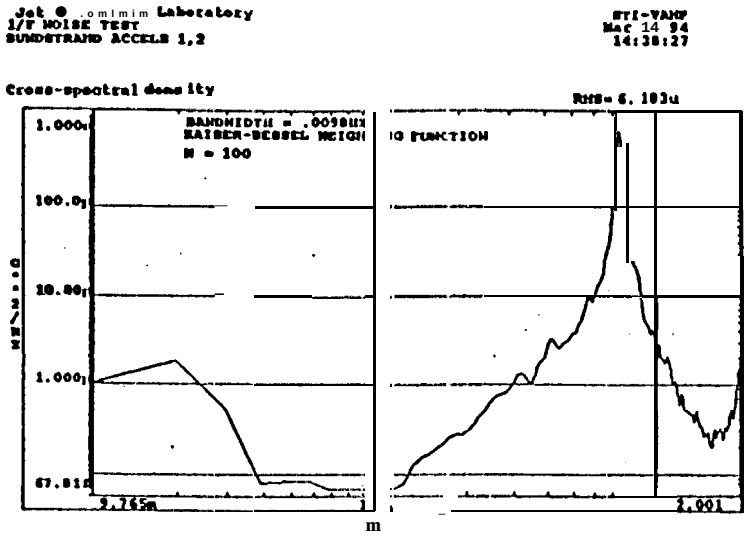

r@m49C

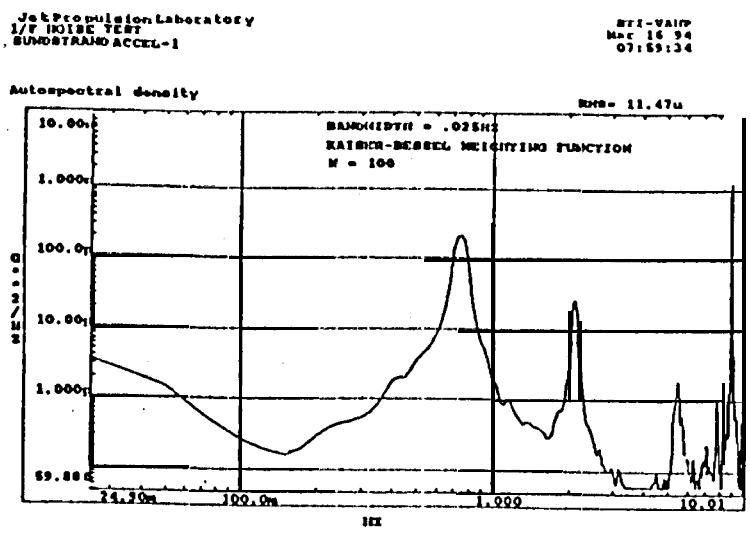

Figure 10A

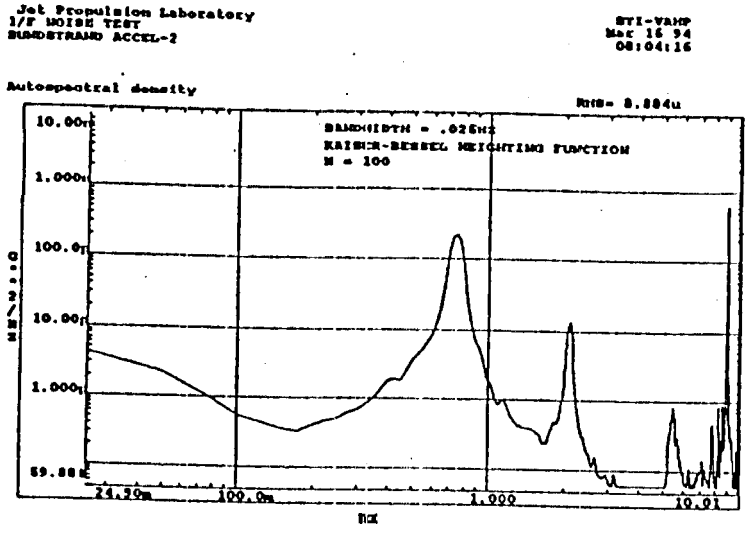

Figure 10B

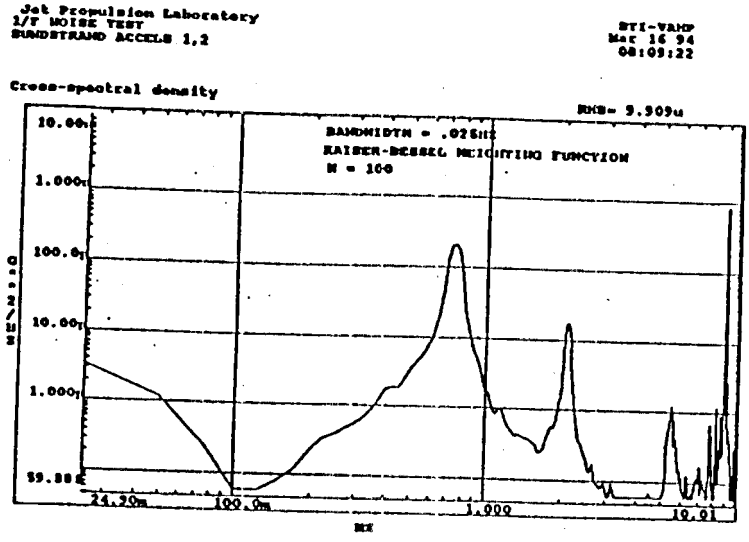

Figure 10C

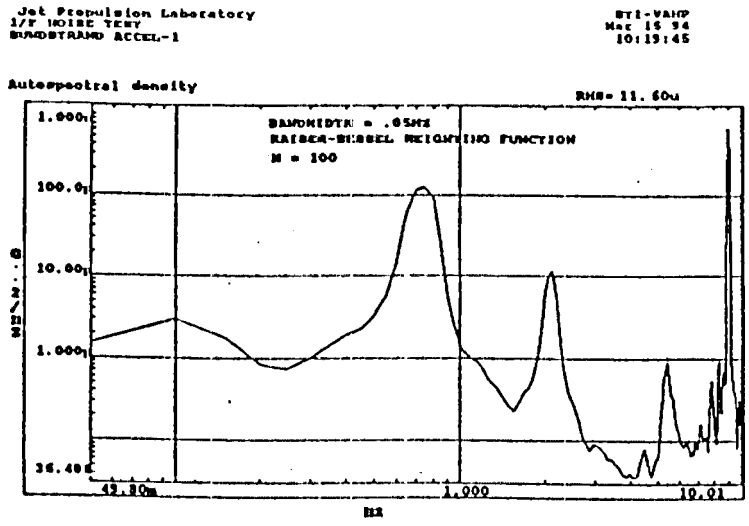

Figure 11A

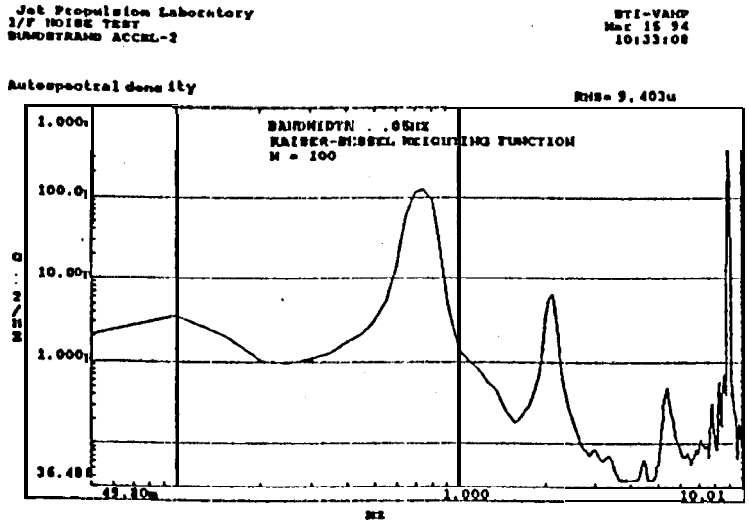

Figure 11B

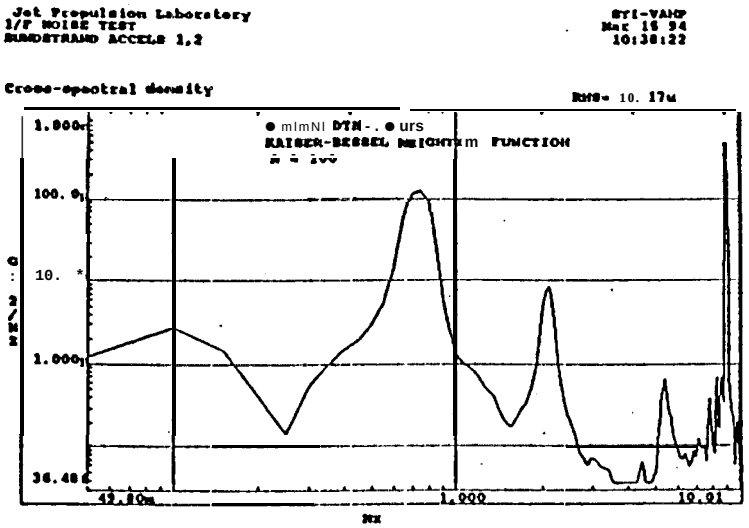

Figure 11C

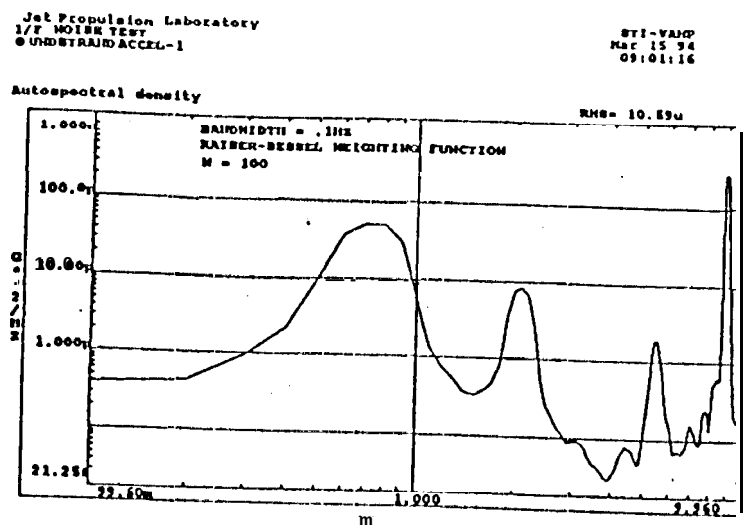

Figure 12A

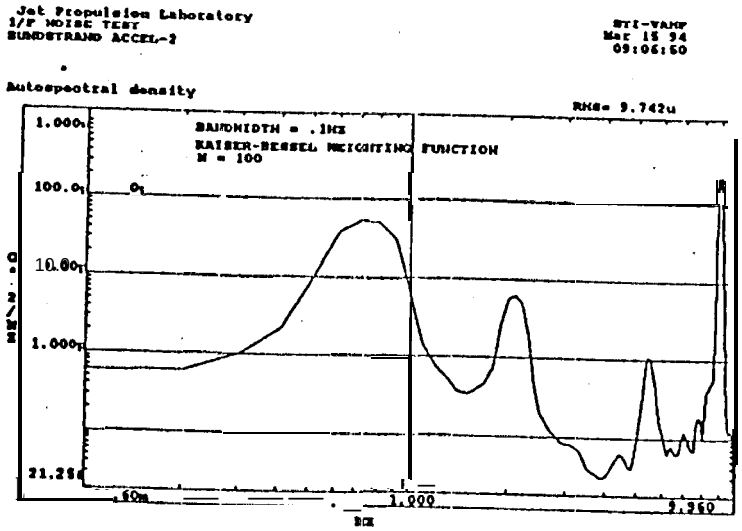

Figure 12B

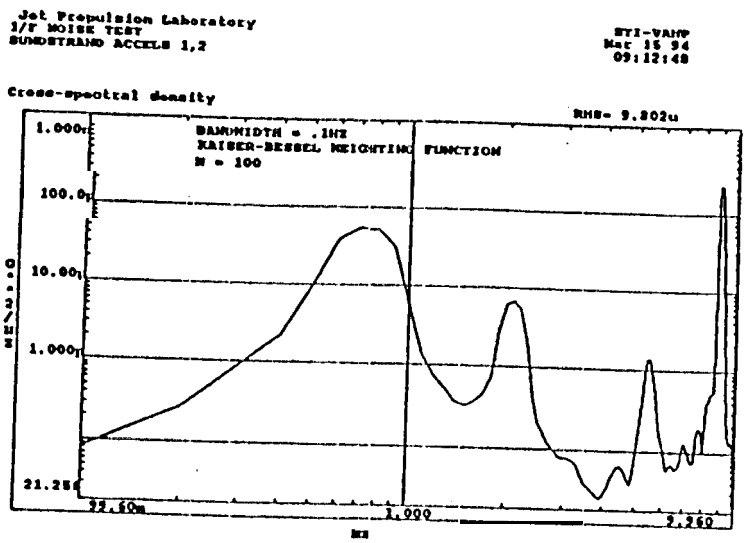

Figure 12C